Int. J. Electrochem. Sci., 17 **(2022)** Article Number: 221133, doi: 10.20964/2022.11.37

International Journal of
ELECTROCHEMICAL
SCIENCE
www.electrochemsci.org

Short Communication

Corrosion resistance of HRB500 steel rebar coated with glass fiber reinforced magnesium phosphate cement composite in 3.5% sodium chloride solution

Yubing Du[1,2,*], *Zhaoyu Wang*[1], *Peiwei Gao*[2], *Yong Yin*[1,3], *Jianming Yang*[1]

[1]School of Civil Engineering, Yancheng Institute of Technology, Yancheng, 224051, China
[2]College of Civil Aviation, Nanjing University of Aeronautics and Astronautics, Nanjing, 210016, China
[3]Yancheng Boyou Transportation Technology Co., Ltd, Yancheng, 224051, China
[*]E-mail: duyubing@126.com

Received: 9 July 2022 / *Accepted:* 13 September 2022 / *Published:* 10 October 2022

Electrochemical impedance spectroscopy and polarization techniques were used to assess the impact of the addition of glass fibers (GFs) in a range of concentrations to magnesium phosphate cement (MPC) on the electrochemical corrosion resistance of HRB500 steel reinforced concrete while it was immersed in a 3.5wt.% NaCl solution to simulate a marine environment. Due to the reduction in water absorption and chloride ion permeability, reinforced concrete containing 4wt% GFs was most successful in improving the corrosion resistance of reinforcement bars. The SEM micrograph of the samples showed that the addition of GFs improved the separation and irregularity structure of the steel rebar. The findings show that the GFs as an admixture improve concert durability and stop corroding ions from penetrating the surfaces of the steel rebars, suggesting that it may be a substitute material in the growth of the construction sector.

Keywords: Glass fibers**;** Corrosion resistance**;** Magnesium phosphate cement**;** Reinforced concrete**;** Electrochemical impedance spectroscopy

1. INTRODUCTION

The major binder in conventional concrete is ordinary Portland cement (OPC) [1, 2]. However, it is well-known that the high embodied energy consumption and CO_2 emissions associated with OPC manufacturing have a detrimental effect on the environment [3-5]. Magnesium phosphate cement (MPC) seems to be a form of chemically bonded ceramic (CBC) that is created when phosphates and magnesium oxide (MgO) combine in an acidic base [6, 7]. MgO reacts with PDP or ADP to form K-struvite or struvite, respectively, as hydration products to create magnesium potassium phosphate

cements and magnesium ammonia cements, which are kinds of MPC [8, 9]. It is also a clinker-free cement in which the mechanism of strength growth occurs as a result of the rapid production of cementitious products of the hydrogel type [10, 11]. The significance of MPC within the categories of elevated materials in the field of civil engineering has been established by earlier studies [12-14].

When chloride ions are present in the environment, steel reinforcing used in infrastructure can corrode and cause cracks in the cement concrete [15, 16]. Through these gaps, oxygen, moisture, and chloride ions may enter the steel reinforcement quickly, accelerating the corrosion process and degrading the concrete [17]. The corrosion that results from this can even cause steel reinforcement in concrete to separate from it [18, 19]. Recently, the use of admixtures has received special attention in construction application, particularly in cement concrete and mortar [20]. Among various manufactured materials, fibers have recently been indicated to advance the stability and microstructure of cement-based systems [21].

Nonetheless, fully protecting all metal rebars in concrete is difficult [22]. According to several studies, using additives in concrete provides the most efficient and straightforward approach to lower building costs, reduce environmental pollution, and increase the durability of concrete [23, 24]. Admixtures are added to concrete to improve its qualities in place of cement [25-27]. Additionally, it can lower concrete density and cut down on CO2 emissions [28-30].

The expansion of concrete reinforced with various fiber types have been the subject of numerous studies, which has improved the material's mechanical and chemical resilience [31, 32]. These characteristics are the essential elements that can support concrete usage in the building industry [33, 34]. Additionally, fiber mixing is an important tactic that may be used to reduce the mechanical and physical constraints of reinforced concrete and expand the scope of its applications [35, 36].

Although glass fibers (GFs) have been shown to enhance the electrical resistivity and reduce the specific surface area and permeability, the effect of GFs on the corrosion resistance of steel rebars has not been previously reported. Hence, this work focused on the effect of GFs in various concentrations in MPC on the corrosion resistance and electrical resistivity of steel rebars.

2. MATERIALS AND METHOD

In a similar way to Portland cement, the MPC was made from a mix of dead-burned MgO, NH4H2PO4, fly ash (FA), and borax in different amounts.

The Taishan-Refractory-Plant in Shanghai provided the powder with a specific surface area of 220 m2/kg and a particle size average of 1.1 lm. It was calcined for 5 hours at approximately 1400 °C, yielding a purity of 92.5%. The borax and ammonium dihydrogen orthophosphate used in this study were of industrial grade. Table 1 displays the chemical make-up of both magnesia and fly ash. In the current work, a glass fiber with a diameter of 9.4 mm and a length of 12 mm was employed. Table 2 lists the glass fiber's physical characteristics.

Table 1. Chemical compositions of MPC and FA

Parameters	**MPC**	**FA**
MgO (%)	89.14	1.76
SiO_2 (%)	4.98	54.74
Al_2O_3 (%)	2.74	25.52
Fe_2O_3 (%)	1.12	6.65
CaO (%)	1.53	8.82
P_2O_3	0.12	-
K_2O (%)	-	0.31
Na_2O (%)	-	0.30
SO_3 (%)	-	0.62
LOI (%)	0.37	1.28

Table 2. Glass fiber's physical characteristics

Properties	
Linear density (dtex)	1.53
Dry density (g/cm^3)	2.5
Breaking strength (MPa)	1510
Modulus of elasticity (GPa)	29.5
Elongation at break (%)	5.4

Each sample contained MgO, $NH_4H_2PO_4$, FA, borax, sand, and glass fiber, and the weight ratio of water to solid (W/C), which was kept at 0.16, was designed for the specimen with fiber volume percentages of 1%, 2%, 3%, and 4%. The samples were made with a constant mixture of borax (3.5% of the mass of metal oxide), with sand/binder ratios of 1:1, 1:1.2, and 1:1.5. It is important to note that glass fiber increases the water needed while the water to solids ratio affects the specimen's strength. When the volume percentage of fiber increases or the cement/sand ratio is less than 1:1, the water reduction (Sodium Polyacrylate, PAAS) must be adjusted in order to maintain the fluidity of the mix and the practicability of the specimen.

In this study, the corrosion resistance of HRB500 steel with a 2 cm diameter was examined. The chemical make-up of HRB500 steel is presented in Table 3.

Table 3. Chemical compositions of HRB500 steel rebar

C	P	Mn	S	Si	Fe
0.20wt%	0.03wt%	1.50wt%	0.025wt%	0.55wt%	Residual

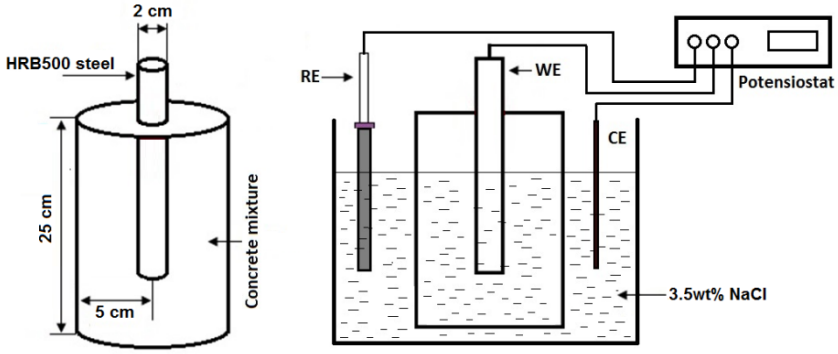

Figure 1. Schematic diagram of the HRB500 steel reinforced MPC used as a working electrode in electrochemical experiments

To make working electrodes, the concrete mixture was poured into a cylindrical mold with a diameter of 10 cm and a height of 25 cm, and a steel rebar was placed vertically in the center. Open circuit potential (OCP) was measured through a high-impedance voltmeter with an input resistance. EIS as nondestructive monitoring techniques were used to study the corrosion behavior of mild steel rebars. An electrochemical procedure was used with the HRB500 steel reinforced MPC, saturated calomel and graphite as the working, reference and counter electrodes, respectively. Figure 1 shows a schematic diagram and detailed dimensions for a reinforced MPC sample. The samples were immersed in the media containing 3.5wt% NaCl. A unique piece of software was used to analyze the results that were produced. Analyses using electrochemical impedance spectroscopy (EIS) were carried out in the 100 kHz to 100 µHz frequency range. The polarization experiment was conducted at a scan rate of 1mV/s starting at 0.25V. As per ASTM C642, water absorption was measured. Using a scanning electron microscope (SEM), the morphological properties of HRB500 steel rebars were studied.

3. RESULTS AND DISCUSSION

The water absorption of MPC with different levels of GFs exposed to 3.5wt% NaCl solution after 2-days, 2-weeks, 1-month and 2-months is revealed in Fig. 2. As shown, all the samples with GFs reveal a decrease in water absorption by rising immersion time compared to the MPC sample. This means that GFs in MPC structures may decrease the water absorption of MPC after being exposed to the marine environment. The MPC specimen with 4% GFs shows lower water absorption compared to the other specimens, displaying a significant effect on water absorption by adding both GFs in MPC.

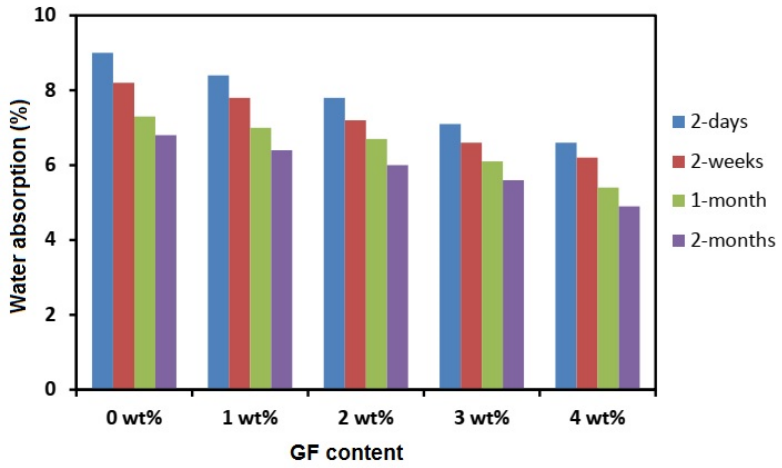

Figure 2. Water absorption of MPC with different level of GFs exposed to 3.5wt% NaCl solution after 2-days, 2-weeks, 1-month and 2-months

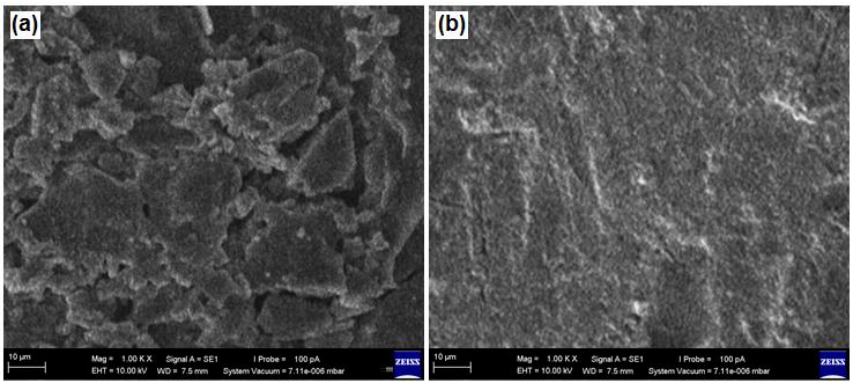

Figure 3. FESEM images of HRB500 steel in MPC specimens with (a) 0 wt% GFs, (b) 4.0 wt% GFs immersed in 3.5% NaCl solution after two months of exposure time at room temperature

Figure 3 displays the FESEM images of HRB500 steel in MPC specimens with 0 wt% GFs and 4.0 wt% GFs immersed in 3.5% NaCl solution after two months of exposure time at room temperature. The surface of rebars in MPC specimens with 4.0 wt% GFs content shows the lowest pits and minor corrosion yields, indicating the slight pitting corrosion shaped onto the surface of HRB500 rebar, which is in accordance with the results attained from water absorption analysis. It may be associated with the reduction of water permeability and Cl^- ion into reinforced MPC samples. The large pores may be altered to lesser pores by the addition of GFs, resulting in an alteration in the structure of MPC [37, 38]. These results reveal that GFs in MPC created a decrease in corrosion rate and enhanced corrosion resistance of HRB500 rebars due to the reduction of water permeability and Cl^- ion [39-41].

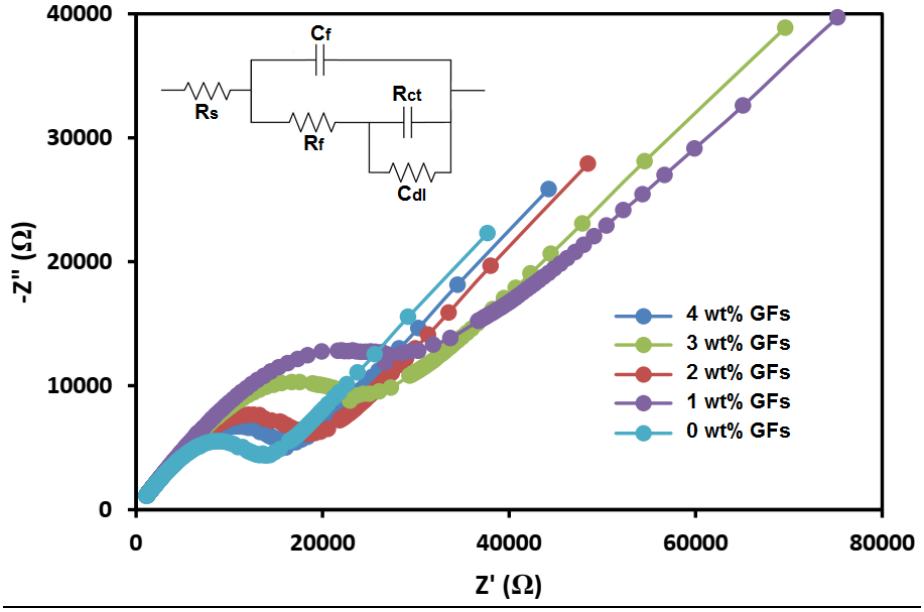

Figure 4. EIS curves of HRB500 steel coated with glass fiber reinforced magnesium phosphate cement composite in 3.5 % NaCl (GF content: 0,1,2,3 and 4%) after 4 weeks of immersion time. Inset figure shows fitted circuit model

Table 4. The attained data for HRB500 steel coated with glass fiber reinforced magnesium phosphate cement composite in 3.5 % NaCl (GF content: 0,1,2,3 and 4%) after 4 weeks of immersion time

Level of GFs	R_s (Ω)	R_f(kΩ)	C_f(μFcm^{-2})	R_{ct}(kΩ)	C_{dl}(μFcm^{-2})
0 wt%	36.5	14.68	19.3	17.54	23.8
1 wt%	42.9	17.49	17.1	21.37	19.8
2 wt%	39.8	18.78	14.8	23.74	18.2
3 wt%	37.3	32.46	12.4	38.96	14.3
4 wt%	43.7	39.53	9.6	49.63	12.4

The EIS method has been utilized for studying corrosion resistance of HRB500 steel coated with glass fiber reinforced magnesium phosphate cement composite in 3.5 % NaCl (GF content: 0,1,2,3 and 4%). The Nyquist curves attained from EIS measurement were revealed in Fig. 4. Inset of Fig. 4 exhibited an equivalent circuit model used in this research. Where R_s presents solution's resistance [42-44]. R_f and C_f show the resistance and capacitance of modified MPC concrete, respectively. R_{ct} and C_{dl} are charge-transfer-resistance and double-layer-capacitance of the HRB500 steel surface, respectively [45-47]. The attained data is revealed in Table 4.

As shown in table 4, with the addition of GFs in the MPC, R_f rises and C_f reduces, which displays an enhancement to the stability, corrosion resistance, and passive layer thickness of the HRB500 steel. Because of their large surface area, GFs can form a strong bond with hydrated cement, which explains why a larger reserve of $Ca(OH)_2$ is growing [48, 49]. These GFs fill up capillary holes and minor cracks and then get constricted into the MPC structure. These factors improve the corrosion resistance of HRB500 rebars in 3.5wt% NaCl media. Furthermore, comparing C_f and C_{dl}, it was

detected that C_{dl} was more than C_f in all specimens, which confirms the formation of a thin passive film [50-52].

In order to explore the passive film development and redox responses of the samples in aggressive media, CV examinations were used. Fig. 5 exhibits the CV plots of HRB500 steel coated with glass fiber reinforced magnesium phosphate cement composite in 3.5 % NaCl (GF content: 0,1,2,3 and 4%). The anodic and cathodic peaks may be seen in Fig. 5.

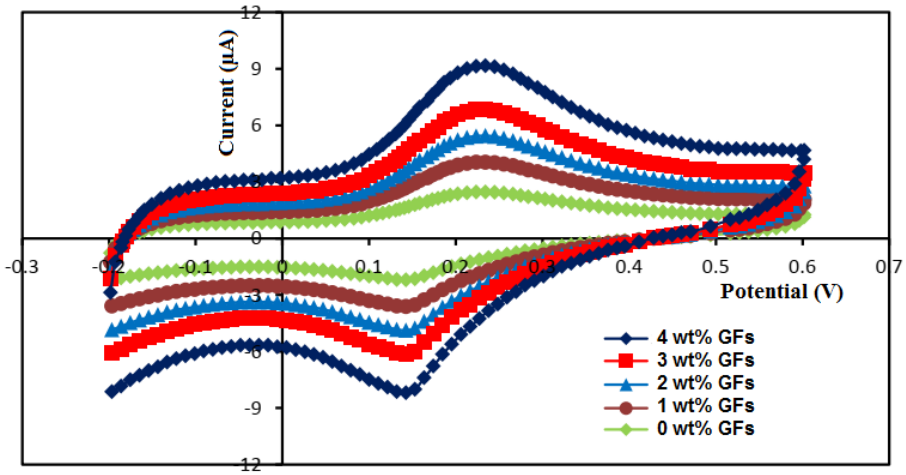

Figure 5. CVs of the HRB500 steel coated with glass fiber reinforced magnesium phosphate cement composite in 3.5 % NaCl (GF content: 0,1,2,3 and 4%) after 4 weeks of immersion time

Anodic peak was seemed at an estimated potential of 0.24V aimed at all samples that is related to alteration starting Fe^{2+} ions toward Fe^{3+} ions and the creation of a passive layer onto the surface of HRB500 rebars.

The current-density values in zero-potential (i_0) can show the corrosion resistance of the passive layer. A greater value suggests lower corrosion resistance [53, 54]. As shown in fig. 5, rebars in MPC specimens with 4.0 wt% GFs content display lower i_0, showing lower corrosion. The reduction in i_0 may be correlated to the steadiness of the passive layers shaped on the HRB500 surface. Figure 5 shows a cathodic peak detected at a potential of 0.13V. When the potential taken moved to a further negative value, the cathodic current-density quickly developed which may be related to electrochemical technique controlled via hydrogen increase.

Polarization curves of HRB500 steel coated with glass fiber reinforced magnesium phosphate cement composite in 3.5% NaCl (GF content: 0,1,2,3, and 4%) are shown in Figure 6. As shown in Fig. 6, all HRB500 rebars have passive areas that are analyzed by an anodic polarization graph, suggesting that the presence of a passive layer on the steel's surface after exposure to a salty environment is clear. Additionally, a massive change in the oxidation potential inside the direction of positivity was observed, showing that the anodic metals dissolving was successfully delayed by altering the concentration of GFs in structural concrete [55, 56].

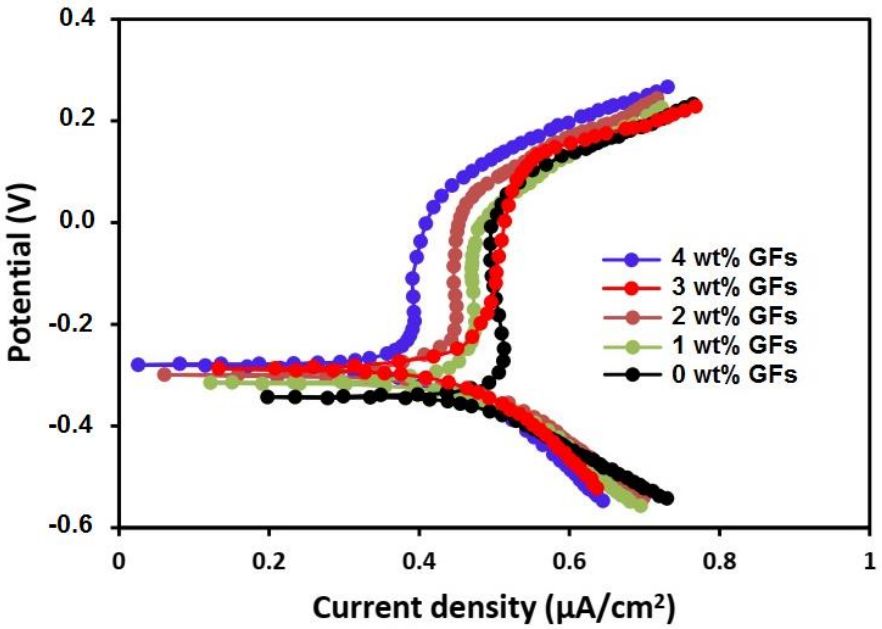

Figure 6. The polarization of HRB500 steel coated with glass fiber reinforced magnesium phosphate cement composite in 3.5 % NaCl (GF content: 0,1,2,3 and 4%) after 4 weeks of immersion time

Table 5. Corrosion parameters attained from polarization plots in Figure 6.

Level of GFs	Corrosion current density($\mu A/cm^2$)	Corrosion potential(V)	$\beta_c(mVdec^{-1})$	$-\beta_a(mVdec^{-1})$
0 wt%	0.52	-0.33	51	31
1 wt%	0.47	-0.31	54	35
2 wt%	0.40	-0.30	57	39
3 wt%	0.42	-0.29	50	44
4 wt%	0.38	-0.27	48	43

The passive region for HRB500 rebars in MPC specimens with 4.0 wt% GFs content was much wider than the other specimens. A further indication of the improved corrosion resistance of HRB500 steel reinforced concrete having GF admixtures is the fact that the passive current density in rebars in MPC specimens with 4.0 wt.% GFs content was lower than that in other specimens. Mechanical properties and durability of concrete structures were improved as a result of the GFs' reaction with free $Ca(OH)_2$ during cement hydration and subsequent formation of calcium silicate hydrate [57, 58]. Table 5 displays the corrosion parameters that were determined from the polarization plots in Figure 6.

The Durar-Network Specification has four levels that can be used to separate the corrosion level. However, the corrosion current-density (i_{corr}) of HRB500 rebars in MPC specimens with 4.0

wt% GFs content in 3.5wt% NaCl media was lower in coparision with other specimens. Therefore, except for the MPC specimen with 0 wt% GFs, all HRB500 steel stayed in a passive condition throughout the electrochemical reaction, demonstrating the material's excellent corrosion resistance in a salty environment [59].

Additionally, as shown in table 5, different concrete samples' cathodic Tafel slopes (β_c) and anodic Tafel slopes (β_a) values fluctuate. It is possible to identify the inhibition of HRB500 steel, the composition of the working electrode, and the charge-transfer coefficient using the change in Tafel slope values. Table 4 demonstrates that the c values in the varied concrete specimens are unchanged, indicating that the cathodic reaction's impact on the hydrogen discharge process is unaltered. The β_a values can, however, alter in different concrete specimens, indicating a blockage in anodic reactive species [60, 61]. Furthermore, the HRB500 rebars' β_a values rise in MPC specimens with a 4.0wt% GFs content, suggesting that the GFs in concrete structures can aid HRB500 steel's ability to resist corrosion in a 3.5 wt% NaCl medium.

Figure 7 indicates corrosion potential for HRB500 steel coated with glass fiber reinforced magnesium phosphate cement composite made by various levels of GFs exposed in 3.5% NaCl at different immersion time. HRB500 steel reinforced concrete showed that the MPC sample including 4wt% GFs indicated a 10% corrosion probability at almost all immersion times. However, MPC sample with 0wt% GFs was shown an uncertain corrosion at all exposure times, showing the slight separation of the passive film or initiation step of pitting corrosion [62].

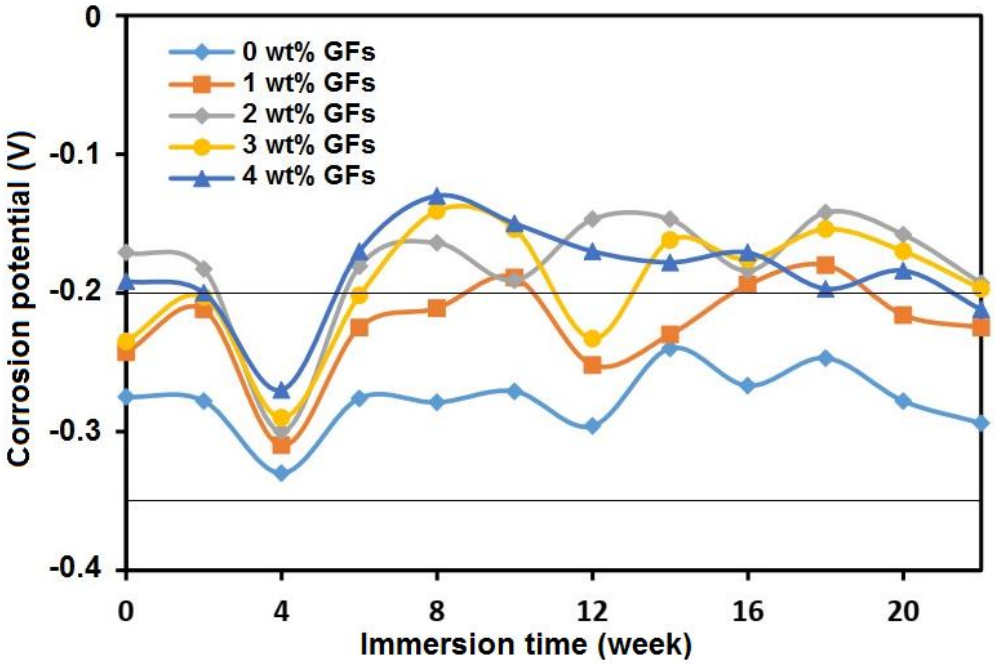

Figure 7. Corrosion potential for HRB500 steel coated with glass fiber reinforced magnesium phosphate cement composite in 3.5 % NaCl (GF content: 0,1,2,3 and 4%) at different immersion time

4. CONCLUSIONS

Corrosion prevention may be possible with a partial substitution for MPC. In this study, the impact of adding GFs to MPC in a range of concentrations on the corrosion resistance of HRB500 steel reinforced concrete was assessed using polarization and EIS techniques while submerged in a 3.5 weight percent NaCl solution to simulate a maritime environment. Due to the reduction in water absorption and chloride ion permeability, reinforced concrete containing 4 wt% GFs was the most successful in improving the corrosion resistance of HRB500 steel rebar. According to the surface properties of the samples, GFs improved the separation and irregularity structures on steel rebars. In a 3.5 wt% NaCl solution, the 4 wt% GFs sample has a lower corrosion current density than the other samples. According to the findings, GFs as an admixture improves concert durability and stops corroding ions from penetrating the surface of HRB500 steel rebars, which can be a substitute material in the development of the construction sector.

ACKNOWLEDGEMENT
The research is supported by the National Nature Science Foundation of China (NSFC) (Grant No. 51578475) and Jiangsu Science and Technology Department (Industry-university-research cooperation project 2020, No. BY2020359).

References

1. A. Sivakrishna, A. Adesina, P. Awoyera and K.R. Kumar, *Materials Today: Proceedings*, 27 (2020) 54.
2. Z. Wu, J. Xu, H. Chen, L. Shao, X. Zhou and S. Wang, *Journal of Materials in Civil Engineering*, 34 (2022) 04022083.
3. G.F. Huseien, A.R.M. Sam, K.W. Shah, J. Mirza and M.M. Tahir, *Construction and Building Materials*, 210 (2019) 78.
4. H. Huang, M. Huang, W. Zhang, S. Pospisil and T. Wu, *Journal of Structural Engineering*, 146 (2020) 04020157.
5. A.A. Mousavi, C. Zhang, S.F. Masri and G. Gholipour, *Structural Health Monitoring*, 21 (2022) 887.
6. B. Yu, J. Zhou, B. Cheng and W. Yang, *Construction and Building Materials*, 283 (2021) 122585.
7. J. Wei, Z. Xie, W. Zhang, X. Luo, Y. Yang and B. Chen, *Engineering Structures*, 230 (2021) 111599.
8. Y. Zhu, Z. Wang, Z. Li and H. Yu, *Journal of Building Engineering*, 45 (2022) 103313.
9. T. Gao, C. Li, D. Jia, Y. Zhang, M. Yang, X. Wang, H. Cao, R. Li, H.M. Ali and X. Xu, *Journal of cleaner production*, 277 (2020) 123328.
10. Y. Liu, B. Chen, Z. Qin, D. Pen and M.A. Haque, *Construction and Building Materials*, 257 (2020) 119570.
11. F.-x. Chen, Y.-c. Zhong, X.-y. Gao, Z.-q. Jin, E.-d. Wang, F.-p. Zhu, X.-x. Shao and X.-y. He, *Scientific Reports*, 11 (2021) 1.
12. Y. Zhu, Z. Wang, Z. Li and H. Yu, *ChemistrySelect*, 5 (2020) 5156.
13. X. Wang, Y. Yang, R. Yang and P. Liu, *Coatings*, 12 (2022) 654.
14. L. Tang, Y. Zhang, C. Li, Z. Zhou, X. Nie, Y. Chen, H. Cao, B. Liu, N. Zhang and Z. Said, *Chinese Journal of Mechanical Engineering*, 35 (2022) 3.

15. F. Qu, W. Li, W. Dong, V.W. Tam and T. Yu, *Journal of Building Engineering*, 35 (2021) 102074.
16. J. Yuan, D. Lei, Y. Shan, H. Tong, X. Fang and J. Zhao, *International Journal of Civil Engineering*, 20 (2022) 763.
17. P. Li, W. Li, Z. Sun, L. Shen and D. Sheng, *Cement and Concrete Composites*, 121 (2021) 104100.
18. D. di Summa, J.R. Tenório Filho, D. Snoeck, P. Van den Heede, S. Van Vlierberghe, L. Ferrara and N. De Belie, *Journal of Cleaner Production*, 358 (2022) 131998.
19. Y. Shan, J. Zhao, H. Tong, J. Yuan, D. Lei and Y. Li, *Soil Dynamics and Earthquake Engineering*, 161 (2022) 107419.
20. S. Gupta, H.W. Kua and C.Y. Low, *Cement and concrete composites*, 87 (2018) 110.
21. F. Zahiri and H. Eskandari-Naddaf, *Frontiers of Structural and Civil Engineering*, 13 (2019) 821.
22. H. Kim, C.-J. Lee, C.-S. Shon, H. Moon and C.-W. Chung, *Journal of Structural Integrity and Maintenance*, 5 (2020) 8.
23. K.A. Aghdam, A.F. Rad, H. Shakeri and J.M. Sardroud, *Journal of Construction Engineering and Project Management*, 8 (3) (2018) 1.
24. X. Wu, C. Li, Z. Zhou, X. Nie, Y. Chen, Y. Zhang, H. Cao, B. Liu, N. Zhang and Z. Said, *The International Journal of Advanced Manufacturing Technology*, 117 (2021) 2565.
25. M.A.M. Langaroudi and Y. Mohammadi, *Construction and building materials*, 191 (2018) 619.
26. F. Chen, Z. Jin, E. Wang, L. Wang, Y. Jiang, P. Guo, X. Gao and X. He, *Scientific Reports*, 11 (2021) 4208
27. Z. Said, S. Arora, S. Farooq, L.S. Sundar, C. Li and A. Allouhi, *Solar Energy Materials and Solar Cells*, 236 (2022) 111504.
28. W. Zhang, X. Liu, Y. Huang and M.-N. Tong, *Archives of Civil and Mechanical Engineering*, 22 (2022) 171.
29. T. Gao, Y. Zhang, C. Li, Y. Wang, Q. An, B. Liu, Z. Said and S. Sharma, *Scientific reports*, 11 (2021) 22535.
30. X. Wang, C. Li, Y. Zhang, H.M. Ali, S. Sharma, R. Li, M. Yang, Z. Said and X. Liu, *Tribology International*, 174 (2022) 107766.
31. N.A. Farhan, M.N. Sheikh and M.N. Hadi, *Journal of Materials in Civil Engineering*, 30 (2018) 04018142.
32. R. Ye, P. Liu, K. Shi and B. Yan, *IEEE access*, 8 (2020) 214346.
33. T.D. Akinosho, L.O. Oyedele, M. Bilal, A.O. Ajayi, M.D. Delgado, O.O. Akinade and A.A. Ahmed, *Journal of Building Engineering*, 32 (2020) 101827.
34. Z. Zhang, Q. Yang, Z. Yu, H. Wang and T. Zhang, *Materials Characterization*, 189 (2022) 111962.
35. D.-M. Ge, L.-C. Zhao and M. Esmaeili-Falak, *Journal of Sustainable Cement-Based Materials*, 12 (2022) doi: 10.1080/21650373.2022.2093291
36. Y. Yang, H. Zhu, X. Xu, L. Bao, Y. Wang, H. Lin and C. Zheng, *Microporous and Mesoporous Materials*, 324 (2021) 111289.
37. C.M. Tibbetts, J.M. Paris, C.C. Ferraro, K.A. Riding and T.G. Townsend, *Cement and Concrete Composites*, 107 (2020) 103491.
38. M. Yang, C. Li, Z. Said, Y. Zhang, R. Li, S. Debnath, H.M. Ali, T. Gao and Y. Long, *Journal of Manufacturing Processes*, 71 (2021) 501.
39. E. Ariyachandra, S. Peethamparan, S. Patel and A. Orlov, *Construction and Building Materials*, 291 (2021) 123328.
40. X. Cui, C. Li, Y. Zhang, Z. Said, S. Debnath, S. Sharma, H.M. Ali, M. Yang, T. Gao and R. Li, *Journal of Manufacturing Processes*, 80 (2022) 273.

41. M. Yang, C. Li, Y. Zhang, Y. Wang, B. Li, D. Jia, Y. Hou and R. Li, *Applied Thermal Engineering*, 126 (2017) 525.
42. A. Fouda, M. Eissa and A. El-Hossiany, *International Journal of Electrochemical Science*, 13 (2018) 11096.
43. G. Li, H. Yuan, J. Mou, E. Dai, H. Zhang, Z. Li, Y. Zhao, Y. Dai and X. Zhang, *Composites Communications*, 29 (2022) 101043.
44. D. Jia, Y. Zhang, C. Li, M. Yang, T. Gao, Z. Said and S. Sharma, *Tribology International*, 169 (2022) 107461.
45. C. Chen, J. Zuo and Y. Wang, *International Journal of Electrochemical Science*, 15 (2020) 1634.
46. Y. Lan, B. Zheng, T. Shi, C. Ma, Y. Liu and Z. Zhao, *Magazine of Concrete Research*, (2022) https://doi.org/10.1680/jmacr.21.00227
47. J. Wang, Q. Meng, Y. Zou, Q. Qi, K. Tan, M. Santamouris and B.-J. He, *Water Research*, 221 (2022) 118755.
48. X. Zhu, D. Tang, K. Yang, Z. Zhang, Q. Li, Q. Pan and C. Yang, *Construction and Building Materials*, 175 (2018) 467.
49. B. Bai, Q. Nie, Y. Zhang, X. Wang and W. Hu, *Journal of Hydrology*, 597 (2021) 125771.
50. T. Shi, Y. Lan, Z. Hu, H. Wang, J. Xu and B. Zheng, *International journal of concrete structures and materials*, 16 (2022) 2.
51. T. Gao, C. Li, Y. Wang, X. Liu, Q. An, H.N. Li, Y. Zhang, H. Cao, B. Liu and D. Wang, *Composite Structures*, 286 (2022) 115232.
52. T. Gao, Y. Zhang, C. Li, Y. Wang, Y. Chen, Q. An, S. Zhang, H.N. Li, H. Cao and H.M. Ali, *Frontiers of Mechanical Engineering*, 17 (2022) 24.
53. J. Michalska, M. Sowa, A. Stolarczyk, F. Warchoł, K. Nikiforow, M. Pisarek, G. Dercz, M. Pogorielov, O. Mishchenko and W. Simka, *Electrochimica Acta*, 419 (2022) 140375.
54. H. Cheng, L. Sun, Y. Wang and X. Chen, *International Journal of Fatigue*, 151 (2021) 106386.
55. J. Hu, S. Zhang, E. Chen and W. Li, *Construction and Building Materials*, 325 (2022) 126718.
56. X. Li, J. Yan, T. Yu and B. Zhang, *Colloids and Surfaces A: Physicochemical and Engineering Aspects*, 642 (2022) 128701.
57. D. Zhao and R. Khoshnazar, *Cement and Concrete Composites*, 122 (2021) 104162.
58. Z. Zhu, W. Yunlong and Z. Liang, *Frontiers in Earth Science*, 10 (2022) 157.
59. S. Znaniecki, K. Szwabińska, J. Wojciechowski, A. Skrzypczak, M. Baraniak and G. Lota, *Electrochemistry Communications*, 23 (2022) 107326.
60. G.Y. Koga, B. Albert, V. Roche and R.P. Nogueira, *Electrochimica Acta*, 261 (2018) 66.
61. T. Shi, Y. Liu, Y. Zhang, Y. Lan, Q. Zhao, Y. Zhao and H. Wang, *International Journal of Concrete Structures and Materials*, 16 (2022) 10.
62. J. Xie, J. Zhang, Z. Zhang, Q. Yang, K. Guan, Y. He, R. Wang, H. Zhang, X. Qiu and R. Wu, *Corrosion Science*, 198 (2022) 110163.